Journal of Materials Chemistry C

PAPER

View Article Online
View Journal | View Issue

Cite this: J. Mater. Chem. C, 2014, 2, 9523

Novel phosphorescent polymers containing both ambipolar segments and functionalized Ir^{III} phosphorescent moieties: synthesis, photophysical, redox, and electrophosphorescence investigation†

Meng Lian,[a] Yue Yu,[b] Jiang Zhao,[a] Zuan Huang,[a] Xiaolong Yang,[a] Guijiang Zhou,*[a] Zhaoxin Wu*[b] and Dongdong Wang*[a]

Received 24th July 2014
Accepted 13th September 2014

DOI: 10.1039/c4tc01626b

www.rsc.org/MaterialsC

Two series of novel phosphorescent polymers have been successfully synthesized by the Suzuki cross-coupling reaction among functionalized phosphorescent Ir^{III} ppy-type (ppy = 2-phenylpyridine anion) complex monomers with hole-injection/transporting (HI/HT) properties, fluorene-based silane moieties and triphenylamine-oxadiazole hybrid units showing ambipolar features. Their photo-physical, electrochemical, and electroluminescent (EL) properties have been investigated. The concerned results have indicated the efficient energy-transfer from the organic segments to the phosphorescent units in the polymer backbone. The electrochemical characterization has shown that introducing the triphenylamine-oxadiazole hybrid blocks can facilitate the injection processes for both kinds of charge carriers and afford ambipolar features to the copolymers. All these features associated with these novel phosphorescent polymers will guarantee their exceptional EL performances, which have been shown by organic light-emitting devices (OLEDs). The OLEDs based on these phosphorescent polymers can furnish a maximum current efficiency (η_L) of 30.54 cd A^{-1}, an external quantum efficiency (η_{ext}) of 12.93%, and a power efficiency (η_P) of 10.12 lm W^{-1}. So, these attractive results will offer a new outlet to afford functionalized phosphorescent polymers for constructing highly efficient OLEDs with low-cost device fabrication.

Introduction

Phosphorescent polymers have received substantial research interest for their application in organic light-emitting devices (OLEDs).[1–5] Compared with their small molecular phosphorescent counterparts, phosphorescent polymers can show the advantages of low-cost fabrication, flexibility, large area, easy device construction, *etc.*[6–10] In order to obtain phosphorescent polymers, the phosphorescent chromophores can be either attached[5,11–19] or imbedded[20–25] into the polymer backbones, which can adopt conjugated[5,11–13] or non-conjugated[14,16,17,26–28] structures. The phosphorescent chromophores adopted in these polymers are typically ppy-type (ppy = 2-phenylpyridine anion) Ir^{III} complexes for their high phosphorescent quantum yield (Φ_P), tunable emission color, and relatively short lifetimes for the triplet states (τ_P). According to the established theory of the energy-level for single and triplet excited states in the organic conjugated systems,[29] the conjugated backbones of the phosphorescent polymers typically possess nonemissive triplet states with low energy-levels. This situation will increase the chance of undesired back energy-transfer from phosphorescent chromophores in the phosphorescent polymers to the non-emissive triplet states associated with their conjugated backbones.[3,22] Hence, the back energy-transfer process will hamper the electroluminescent (EL) process of the concerned phosphorescent polymers. With the aim to deal with this problem, phosphorescent polymers with nonconjugated backbones have been developed through bonding the phosphorescent units to side chains of the nonconjugated polymers.[14,16,17,26–28] Unfortunately, the nonconjugated backbones will do harm to the charge carrier injection/transporting ability which is very critical to the EL process. Additionally, the alkyl groups which afford

[a]MOE Key Laboratory for Nonequilibrium Synthesis and Modulation of Condensed Matter, State Key Laboratory for Mechanical Behavior of Materials, Institute of Chemistry for New Energy Materials, Department of Chemistry, Faculty of Science, Xi'an Jiaotong University, Xi'an 710049, P. R. China. E-mail: zhougj@mail.xjtu.edu.cn; Fax: +86-29-8266-3914

[b]Key Laboratory of Photonics Technology for Information School of Electronic and Information Engineering, Xi'an Jiaotong University, Xi'an 710049, P. R. China. E-mail: zhaoxinwu@mail.xjtu.edu.cn; Fax: +86-29-82664867

† Electronic supplementary information (ESI) available: Synthetic details of some organic compounds, PL spectra for the polymer solution, EL spectra for devices **G1–G4**, and some electroluminescent data for the concerned devices. See DOI: 10.1039/c4tc01626b

solubility to phosphorescent polymers will disfavor the charge carrier injection/transporting process as well. So, functional groups have been introduced into either the backbones or side chains of the phosphorescent polymers to improve their charge carrier injection/transporting properties.[12,14,16,17,26–28]

Recently, it has been shown that functionalizing should represent an important strategy for improving the EL performance of phosphorescent emitters through enhancing their charge carrier injection/transporting ability.[30–37] So, functional groups with both hole injection/transporting (HI/HT) properties (triphenylamine, carbazole, *etc.*) and electron injection/transporting (EI/ET) characters (aromatic borane, diphenylphosphoryl group, *etc.*) have been employed to develop highly efficient phosphorescent emitters.[30,37] Furthermore, ambipolar host materials have also been developed to fulfill balanced injection/transporting for both kinds of charge carriers and hence increase their recombination efficiency.[38–40] So, ambipolar hosts can effectively enhance the EL efficiency of phosphorescent emitters as well. Obviously, these new strategies should provide valuable information for designing novel phosphorescent polymers which can cope with the problems associated with the traditional analogs. Bearing this in mind, we have designed and prepared new phosphorescent polymers with both triphenylamine functionalized phosphorescent chromophores and ambipolar triphenylamine-oxadiazole hybrid units. Furthermore, fluorene-based silane blocks have also been introduced to the backbones of the new polymers with the aim to increase their triplet energy and relieve the trouble of back energy-transfer and bring high EL efficiencies.

Experimental

General information

All reactions were carried out under a nitrogen atmosphere. The solvents were purified by routine procedures and distilled under dry nitrogen before use. All commercially available reagents were used as received unless otherwise stated. The reactions were monitored by thin-layer chromatography (TLC) with Merck pre-coated aluminum plates. Flash column chromatography and preparative TLC were carried out using silica gel. All Suzuki copolymerization reactions were carried out with Schlenk techniques in an inert atmosphere.

Physical measurements

^{1}H-NMR and ^{13}C-NMR spectra were measured in $CDCl_3$ or DMSO-d_6 with a Bruker AXS 400 MHz spectrometer with the chemical shifts quoted relative to tetramethylsilane (TMS). Fast atom bombardment (FAB) mass spectra were recorded on a Finnigan MAT SSQ710 system. UV-vis spectra were recorded with a Shimadzu UV-2250 spectrophotometer. The photoluminescent (PL) properties of the copolymers were measured with an Edinburgh Instruments FLS920 fluorescence spectrophotometer. With the aim to obtain the triplet energy-level, the 77 K PL spectra were obtained by dipping the degassed sample CH_2Cl_2 solution (*ca.* 0.02 mg mL^{-1}) in a thin quartz tube into a liquid nitrogen Dewar and recorded the PL spectra after 5 minutes of standing. In order to avoid the interference from the singlet emission signal, the 77 K PL spectrum for the pure organic sample was obtained with highly dilute solution. The lifetimes for the excited states were measured using a single photon counting spectrometer from Edinburgh Instruments FLS920 with a 400 nm picosecond LED lamp as the excitation source. The data analysis was conducted by the iterative convolution of the luminescence decay profile with the instrument response function using the software package provided by Edinburgh Instruments. Differential scanning calorimetry (DSC) was performed with a NETZSCH DSC 200 PC unit under a nitrogen flow at a heating rate of 10 °C min^{-1}. Thermogravimetric analysis (TGA) was conducted with a NETZSCH STA 409C instrument under nitrogen with a heating rate of 20 °C min^{-1}. The molecular weights of the copolymers were determined by Waters 2695 GPC in THF. The number-average and weight-average molecular weights were estimated by using a calibration curve of polystyrene standards. Cyclic voltammetry (CV) measurement for the sample solution was performed on a Princeton Applied Research model 2273A potentiostat with a glassy carbon working electrode, a platinum counter electrode, and a platinum-wire reference electrode at a scan rate of 100 mV s^{-1}. The solvent was deoxygenated dichloromethane, and the supporting electrolyte was 0.1 M [nBu$_4$N][BF$_4$]. Ferrocene (Fc) was added as an internal calibrant for the measurement, and all potentials reported were quoted with reference to the Fc–Fc$^+$ couple. The oxidation (E_{ox}) and reduction (E_{red}) potentials were used to determine the HOMO and LUMO energy levels of the polymers by using the equations $E_{HOMO} = -(E_{ox} + 4.8)$ eV and $E_{LUMO} = -(E_{red} + 4.8)$ eV, which were calculated by using the internal-standard ferrocene value of −4.8 eV with respect to the vacuum level.

Materials and synthesis

The compounds **Tz-Am**,[41] **Py-Am**,[30] **BP**,[40] and 2,7-dibromo-9,9-dibutylfluorene[42] were synthesized according to the published procedures. Thallium(I)acetonacetate ([Tl(acac)]) was purchased from Aldrich.

L1. To the solution of **Tz-Am** (0.38 g, 1.00 mmol) in $CHCl_3$ (30 mL), NBS (0.185 g, 1.05 mmol) was added slowly at 0 °C. After addition, the reaction mixture was stirred overnight. Then, the solution was washed with water (2 × 50 mL). The organic layer was dried over anhydrous $MgSO_4$. Then the solvent was removed and the residue was purified by silica gel chromatography eluted with CH_2Cl_2–petroleum ether (b.p. 60–90 °C) (1 : 1, v/v) to get the product as a pale yellow solid (0.39 g, 86%). ^{1}H NMR (400 MHz, $CDCl_3$, δ, ppm): 8.02 (d, J = 8.4 Hz, 1H), 7.93 (d, J = 8.4 Hz, 2H), 7.88 (d, J = 8 Hz, 1H), 7.47 (t, J = 7.6 Hz, 1H), 7.41–7.38 (m, 2H), 7.36–7.30 (m, 3H), 7.15–7.09 (m, 5H), 7.03 (d, J = 8.4 Hz, 2H). ^{13}C NMR (100 MHz, $CDCl_3$, δ, ppm): 167.60, 154.24, 149.88, 146.50, 146.08, 134.82, 132.49, 129.65, 128.62, 127.18, 126.41, 126.23, 125.44, 124.82, 124.42, 122.82, 122.19, 121.51, 116.36. FAB-MS (m/z): 456, 458 [M]$^+$. Elemental analysis calcd. (%) for $C_{25}H_{17}BrN_2S$: C 65.65, H 3.75, N 6.12; found: C 65.39, H 3.85, N 6.09.

L2. It was prepared from **Py-Am** (0.32 g, 1.00 mmol) and NBS (0.185 g, 1.05 mmol) in $CHCl_3$ (30 mL), following the same

procedure as for **L1**. The product was obtained as a pale yellow solid (0.35 g, 87%). ^{1}H NMR (400 MHz, $CDCl_3$, δ, ppm): 8.65 (d, J = 4.4 Hz, 1H), 7.87 (d, J = 8.4 Hz, 2H), 7.75–7.70 (m, 1H), 7.67 (d, J = 8 Hz, 1H), 7.36 (d, J = 8.4 Hz, 2H), 7.32 (d, J = 16 Hz, 2H), 7.19 (t, J = 6.4 Hz, 1H), 7.13 (t, J = 8.4 Hz, 4H), 7.07 (t, J = 7.2 Hz, 1H), 7.01 (d, J = 8.4 Hz, 2H). ^{13}C NMR (100 MHz, $CDCl_3$): δ (ppm) 156.93, 149.64, 148.17, 147.04, 146.66, 136.71, 133.75, 132.28, 129.48, 127.89, 125.72, 124.87, 123.70, 123.58, 121.63, 119.96, 115.40. FAB-MS (m/z): 400, 402 $[M]^+$. Elemental analysis calcd. (%) for $C_{23}H_{17}BrN_2$: C 68.84, H 4.27, N 6.98; found: C 68.93, H 4.32, N 6.76.

Ir-M1. Under an N_2 atmosphere, the organic ligand **L1** (0.46 g, 1.00 mmol) and $IrCl_3 \cdot nH_2O$ (160 mg, 60 wt% Ir content) were heated to 110 °C in a mixture of 2-ethoxyethanol and water (3 : 1, v/v) for 16 h. Then the reaction mixture was cooled to room temperature and water was added. The cyclometalated Ir(III) μ-chloro-bridged dimer was formed as a precipitate which was collected and dried under vacuum. The dimer and [Tl(acac)] (0.30 g, 1.00 mmol) were added to CH_2Cl_2 under an N_2 atmosphere. The reaction mixture was allowed to stir at room temperature for 12 h. After that, the solvent was removed under vacuum. The residue was purified by column chromatography using CH_2Cl_2–petroleum ether (b.p. 60–90 °C) (1 : 1, v/v) as the eluent to obtain the product as an orange solid (0.27 g, 45%). ^{1}H NMR (400 MHz, $CDCl_3$, δ, ppm): 7.87–7.85 (m, 2H), 7.75–7.73 (m, 2H), 7.37–7.35 (m, 6H), 7.08 (t, J = 7.6 Hz, 4H), 7.01 (d, J = 8.9 Hz, 4H), 6.97–6.91 (m, 6H), 6.69 (d, J = 8.8 Hz, 4H), 6.47–6.45 (m, 2H), 5.78 (d, J = 2.0 Hz, 2H), 5.14 (s, 1H), 1.78 (s, 6H). FAB-MS (m/z): 1202 $[M]^+$. Elemental analysis calcd. (%) for $C_{55}H_{39}Br_2IrN_4O_2S_2$: C 54.86, H 3.26, N 4.65; found: C 54.69, H 3.48, N 4.39.

Ir-M2. It was prepared from **L2** (0.40 g, 1.00 mmol), $IrCl_3 \cdot nH_2O$ (160 mg, 60 wt% Ir content) and [Tl(acac)] (0.30 g, 1.00 mmol), following the same procedure as for **Ir-M1**. The product was obtained as a yellow solid (0.22 g, 40%). ^{1}H NMR (400 MHz, $CDCl_3$, δ, ppm): 8.25 (d, J = 4.4 Hz, 2H), 7.46 (d, J = 4.0 Hz, 4H), 7.31 (d, J = 8.4 Hz, 2H), 7.24–7.14 (m, 8H), 6.98–6.92 (m, 6H), 6.86–6.84 (m, 2H), 6.77–6.70 (m, 4H), 6.51–6.48 (m, 2H), 5.65 (d, J = 2.4 Hz, 2H), 5.25 (s, 1H), 1.79 (s, 6H). ^{13}C NMR (100 MHz, $CDCl_3$, δ, ppm): 184.53, 167.51, 147.93, 147.79, 147.11, 146.80, 146.64, 138.83, 136.16, 131.74, 128.99, 126.67, 125.75, 125.07, 124.22, 123.06, 120.27, 117.91, 114.95, 114.18, 100.53, 28.87. FAB-MS (m/z): 1090 $[M]^+$. Elemental analysis calcd. (%) for $C_{51}H_{39}Br_2IrN_4O_2$: C 56.10, H 3.60, N 5.13; found: C 55.93, H 3.39, N 5.09.

BP-Br. NBS (0.26 g, 1.46 mmol) was added slowly into a solution of **BP** (0.50 g, 0.71 mmol) in $CHCl_3$ (100 mL), and then stirred at 0 °C for 24 h. The solution was washed with water (2 × 100 mL), and the organic layer was dried over anhydrous $MgSO_4$. The solvent was removed under reduced pressure and the residue was purified by silica gel chromatography eluted with CH_2Cl_2 to get the title compound as a pale yellow solid (0.58 g, 95%). ^{1}H NMR (400 MHz, $CDCl_3$, δ, ppm): 8.21 (d, J = 8.4 Hz, 4H), 7.74 (d, J = 8.4 Hz, 4H), 7.55 (d, J = 8.8 Hz, 4H), 7.30 (t, J = 8 Hz, 4H), 7.15 (t, J = 8.4 Hz, 8H), 7.09 (t, J = 7.2 Hz, 2H), 7.02 (d, J = 8.8 Hz, 4H). ^{13}C NMR (100 MHz, $CDCl_3$, δ, ppm): 164.51, 147.60, 147.00, 146.61, 143.72, 133.81, 132.35, 129.56, 127.98, 127.44, 127.11, 125.74, 124.90, 123.82, 123.78, 122.24, 115.52. FAB-MS (m/z): 866 $[M]^+$. Elemental analysis calcd. (%) for $C_{50}H_{34}Br_2N_4O_2$: C 69.29, H 3.95, N 6.46; found: C 69.21, H 4.15, N 6.39.

FlSi-Br. The solution of 2,7-dibromo-9,9-dibutylfluorene (2.00 g, 4.60 mmol) in THF was treated with 1.66 mL of nBuLi (4.15 mmol) slowly under an N_2 atmosphere at −78 °C. The mixture was stirred for 30 min at −78 °C. Then, dichlorodiphenylsilane (0.44 mL, 2.08 mmol) was added and the mixture was stirred for an additional 1.5 h at −78 °C. After warming to room temperature, the solution was stirred overnight. The reaction was quenched with water, extracted with CH_2Cl_2 and dried over anhydrous $MgSO_4$. Then the solvent was removed and the residue was purified by silica gel chromatography eluted with petroleum ether (b.p. 60–90 °C) and CH_2Cl_2–petroleum ether (2 : 1, v/v) to get the product as a white solid (1.20 g, 65%). ^{1}H NMR (400 MHz, $CDCl_3$, δ, ppm): 7.66–7.57 (m, 10H), 7.45 (t, J = 8.8 Hz, 8H), 7.37 (t, J = 7.2 Hz, 4H), 1.97–1.85 (m, 8H), 1.13–1.04 (m, 8H), 0.71 (t, J = 7.2 Hz, 12H), 0.65–0.56 (m, 8H). ^{13}C NMR (100 MHz, $CDCl_3$, δ, ppm): 153.24, 149.41, 141.55, 139.85, 136.28, 135.24, 134.73, 133.01, 130.79, 129.98, 129.63, 127.84, 126.19, 121.49, 121.38, 119.32, 55.28, 39.82, 25.99, 22.94, 13.85. FAB-MS (m/z): 892 $[M]^+$. Elemental analysis calcd. (%) for $C_{54}H_{58}Br_2Si$: C 72.47, H 6.53; found: C 72.29, H 6.65.

FlSi-B. The mixture of **FlSi-Br** (0.40 g, 0.45 mmol), bis(pinacolato)diborate (0.34 g, 1.34 mmol), KOAc (0.26 g, 2.60 mmol), $Pd(dppf)_2Cl_2$ (0.036 g, 0.038 mmol), and dry 1,4-dioxane (15 mL) was heated at 100 °C for 16 h. After cooling to room temperature, the mixture was filtered and washed with ethyl acetate (3 × 20 mL). The organic phase was dried over $MgSO_4$. Then the solvent was removed and the residue was purified by silica gel chromatography eluted with CH_2Cl_2–petroleum ether (b.p. 60–90 °C) (2 : 1, v/v) to get the product as a white solid (0.27 g, 60%). ^{1}H NMR (400 MHz, $CDCl_3$, δ, ppm): 7.81 (d, J = 8.0 Hz, 2H), 7.75 (s, 2H), 7.71 (t, J = 7.6 Hz, 4H), 7.66 (s, 2H), 7.61 (d, J = 6.8 Hz, 4H), 7.47 (d, J = 7.6 Hz, 2H), 7.43 (d, J = 7.6 Hz, 2H), 7.36 (t, J = 7.2 Hz, 4H), 1.98–1.92 (m, 8H), 1.39 (s, 24H), 1.09–1.02 (m, 8H), 0.68 (t, J = 7.2 Hz, 12H), 0.64–0.58 (m, 8H). ^{13}C NMR (100 MHz, $CDCl_3$, δ, ppm): 150.35, 150.19, 143.86, 142.40, 136.32, 136.60, 135.02, 134.99, 133.69, 133.05, 130.94, 129.52, 128.88, 127.79, 119.66, 119.31, 83.73, 54.98, 39.82, 26.02, 24.93, 23.00, 13.89. FAB-MS (m/z): 988 $[M]^+$. Elemental analysis calcd. (%) for $C_{66}H_{82}B_2O_4Si$: C 80.15, H 8.36; found: C 80.03, H 8.69.

P-O-1. Under an N_2 atmosphere, **Ir-M1** (2.0 mg, 0.0017 mmol), **BP-Br** (42.3 mg, 0.0489 mmol), **FlSi-B** (50 mg, 0.0506 mmol), Na_2CO_3 (0.13 g, 1.23 mmol), and $Pd(PPh_3)_4$ (9.24 mg, 0.008 mmol) were mixed in a solvent mixture of degassed toluene/THF/H_2O (5.0 mL/5.0 mL/1.25 mL). The mixture was vigorously stirred for 48 h at 100 °C. The reaction mixture was then stirred at 100 °C for 12 h after adding phenylboronic acid (3.0 mg, 0.025 mmol), and then stirred at 100 °C for a further 12 h after adding bromobenzene (4.0 mg, 0.025 mmol). After adding water (20 mL), the mixture was extracted with CH_2Cl_2 (3 × 25 mL) and the organic phase was dried over anhydrous Na_2SO_4. Then the solvent was removed and the residue was redissolved in CH_2Cl_2 and purified with a 0.45 μm PTFE syringe filter. After concentration, the copolymer was purified by

precipitation twice in methanol and washed with acetone in a Soxhlet apparatus for 72 h, and dried under vacuum. It was obtained as a light orange solid (yield: 64%). ^{1}H NMR (400 MHz, $CDCl_3$, δ, ppm): 8.20 (d), 7.77–7.01 (m), 1.98–1.95 (m), 1.15–1.06 (m), 0.71–0.67 (m); gel permeation chromatography (GPC): number-average molecular weight (M_n) = 3.5×10^4 g mol^{-1} and polydispersity index (PDI) = 2.1 (against polystyrene standards).

P-O-2. It was prepared from **Ir-M1** (4.0 mg, 0.0033 mmol), **BP-Br** (40.9 mg, 0.0473 mmol), **FlSi-B** (50 mg, 0.0506 mmol), Na_2CO_3 (0.13 g, 1.23 mmol), and $Pd(PPh_3)_4$ (9.24 mg, 0.008 mmol), following the same procedure as for **P-O-1**. The copolymer was obtained as an orange solid (yield: 76%). ^{1}H NMR (400 MHz, $CDCl_3$, δ, ppm): 8.20 (d), 7.77–6.99 (m), 5.11 (s), 2.03–1.91 (m), 1.77 (s), 1.13–1.06 (m), 0.72–0.66 (m); GPC: $M_n = 3.3 \times 10^4$ g mol^{-1} and PDI = 2.2 (against polystyrene standards).

P-O-3. It was prepared from **Ir-M1** (6.0 mg, 0.0050 mmol), **BP-Br** (39.4 mg, 0.0456 mmol), **FlSi-B** (50 mg, 0.0506 mmol), Na_2CO_3 (0.13 g, 1.23 mmol), and $Pd(PPh_3)_4$ (9.24 mg, 0.008 mmol), following the same procedure as for **P-O-1**. The copolymer was obtained as an orange solid (yield: 86%). ^{1}H NMR (400 MHz, $CDCl_3$, δ, ppm): 8.20 (d), 7.75–6.99 (m), 5.15 (s), 2.00–1.92 (m), 1.76 (s), 1.11–1.08 (m), 0.75–0.67 (m); GPC: $M_n = 3.1 \times 10^4$ g mol^{-1} and PDI = 2.5 (against polystyrene standards).

P-O-4. It was prepared from **Ir-M1** (8.0 mg, 0.0067 mmol), **BP-Br** (37.9 mg, 0.0439 mmol), **FlSi-B** (50 mg, 0.0506 mmol), Na_2CO_3 (0.13 g, 1.23 mmol), and $Pd(PPh_3)_4$ (9.24 mg, 0.008 mmol), following the same procedure as for **P-O-1**. The copolymer was obtained as an orange solid (yield: 81%). ^{1}H NMR (400 MHz, $CDCl_3$, δ, ppm): 8.20 (d), 7.77–6.91 (m), 5.14 (s), 1.98–1.91 (m), 1.76 (s), 1.14–1.08 (m), 0.74–0.67 (m); GPC: $M_n = 2.4 \times 10^4$ g mol^{-1} and PDI = 2.2 (against polystyrene standards).

P-G-1. It was prepared from **Ir-M2** (2.0 mg, 0.0018 mmol), **BP-Br** (43.1 mg, 0.0487 mmol), **FlSi-B** (50 mg, 0.0506 mmol), Na_2CO_3 (0.13 g, 1.23 mmol), and $Pd(PPh_3)_4$ (9.24 mg, 0.008 mmol), following the same procedure as for **P-O-1**. The copolymer was obtained as a yellow solid (yield: 62%). ^{1}H NMR (400 MHz, $CDCl_3$, δ, ppm): 8.22 (d), 7.79–7.08 (m), 5.12 (s). 1.98 (t), 1.70 (s), 1.12–1.07 (m), 0.73–0.62 (m); GPC: $M_n = 2.1 \times 10^4$ g mol^{-1} and PDI = 2.0 (against polystyrene standards).

P-G-2. It was prepared from **Ir-M2** (4.0 mg, 0.0037 mmol), **BP-Br** (40.4 mg, 0.0468 mmol), **FlSi-B** (50 mg, 0.0506 mmol), Na_2CO_3 (0.13 g, 1.23 mmol), and $Pd(PPh_3)_4$ (9.24 mg, 0.008 mmol), following the same procedure as for **P-O-1**. The copolymer was obtained as a yellow solid (yield: 82%). ^{1}H NMR (400 MHz, $CDCl_3$, δ, ppm): 8.20 (d), 7.76–7.05 (m), 5.11 (s), 1.98 (t), 1.68 (s), 1.09–1.07 (m), 0.72–0.66 (m); GPC: $M_n = 2.4 \times 10^4$ g mol^{-1} and PDI = 1.9 (against polystyrene standards).

P-G-3. It was prepared from **Ir-M2** (6.0 mg, 0.0055 mmol), **BP-Br** (38.9 mg, 0.0450 mmol), **FlSi-B** (50 mg, 0.0506 mmol), Na_2CO_3 (0.13 g, 1.23 mmol), and $Pd(PPh_3)_4$ (9.24 mg, 0.008 mmol), following the same procedure as for **P-O-1**. The copolymer was obtained as a yellow solid (yield: 83%). ^{1}H NMR (400 MHz, $CDCl_3$, δ, ppm): 8.20 (d), 7.77–6.99 (m), 5.20 (s), 1.98 (t), 1.81 (s), 1.09–1.06 (m), 0.72–0.67 (m); GPC: $M_n = 2.1 \times 10^4$ g mol^{-1} and PDI = 2.0 (against polystyrene standards).

P-G-4. It was prepared from **Ir-M2** (8.0 mg, 0.0073 mmol), **BP-Br** (37.3 mg, 0.0432 mmol), **FlSi-B** (50 mg, 0.0506 mmol), Na_2CO_3 (0.13 g, 1.23 mmol), and $Pd(PPh_3)_4$ (9.24 mg, 0.008 mmol), following the same procedure as for **P-O-1**. The copolymer was obtained as a yellow solid (yield: 71%). ^{1}H NMR (400 MHz, $CDCl_3$, δ, ppm): 8.21 (d), 7.79–7.08 (m), 5.24 (s), 1.98 (t), 1.82 (s), 1.10–1.06 (m), 0.72–0.69 (m); GPC: $M_n = 1.7 \times 10^4$ g mol^{-1} and PDI = 2.3 (against polystyrene standards).

P-OSi. Under an N_2 atmosphere, **Ir-M1** (12.0 mg, 0.01 mmol), **FlSi-Br** (64.0 mg, 0.0717 mmol), **FlSi-B** (80.8 mg, 0.0817 mmol), Na_2CO_3 (0.78 g, 7.38 mmol), and $Pd(PPh_3)_4$ (55.44 mg, 0.056 mmol) were mixed in a solvent mixture of degassed toluene/THF/H_2O (10.0 mL/10.0 mL/2.5 mL). The mixture was vigorously stirred for 48 h at 100 °C. The reaction mixture was then stirred at 100 °C for 12 h after adding phenylboronic acid (18.0 mg, 0.15 mmol), and then stirred at 100 °C for a further 12 h after adding bromobenzene (24.0 mg, 0.15 mmol). After adding water (40 mL), the mixture was extracted with CH_2Cl_2 (3 × 30 mL) and the organic phase was dried over anhydrous Na_2SO_4. Then the solvent was removed and the residue was redissolved in CH_2Cl_2 and purified using a 0.45 μm PTFE syringe filter. After concentration, the copolymer was purified by precipitation twice in methanol and washed with acetone in a Soxhlet apparatus for 72 h, and dried under vacuum. It was obtained as a light orange solid (yield: 82%). ^{1}H NMR (400 MHz, $CDCl_3$, δ, ppm): 7.82–7.62 (m), 7.53–7.41 (m), 7.39–7.36 (m), 5.13 (s), 2.01–1.86 (m), 1.76 (s), 1.13–1.04 (m), 0.75–0.57 (m); gel permeation chromatography (GPC): number-average molecular weight (M_n) = 2.9×10^4 g mol^{-1} and polydispersity index (PDI) = 2.4 (against polystyrene standards).

P-Org. Under an N_2 atmosphere, **BP-Br** (43.7 mg, 0.0506 mmol), **FlSi-B** (50 mg, 0.0506 mmol), Na_2CO_3 (0.13 g, 1.23 mmol), and $Pd(PPh_3)_4$ (9.24 mg, 0.008 mmol) were mixed in a solvent mixture of degassed toluene/THF/H_2O (5.0 mL/5.0 mL/1.25 mL). The mixture was vigorously stirred for 48 h at 100 °C. The reaction mixture was then stirred at 100 °C for 12 h after adding phenylboronic acid (3.0 mg, 0.025 mmol), and then stirred at 100 °C for a further 12 h after adding bromobenzene (4.0 mg, 0.025 mmol). After adding water (20 mL), the mixture was extracted with CH_2Cl_2 (3 × 25 mL) and the organic phase was dried over anhydrous Na_2SO_4. Then the solvent was removed and the residue was redissolved in CH_2Cl_2 and purified using a 0.45 μm PTFE syringe filter. After concentration, the copolymer was purified by precipitation twice in methanol and washed with acetone in a Soxhlet apparatus for 72 h, and dried under vacuum. It was obtained as a pale yellow solid (yield: 87%). ^{1}H NMR (400 MHz, $CDCl_3$, δ, ppm): 8.21 (d), 7.76–7.01 (m), 1.98–1.94 (m), 1.11–1.09 (m), 0.75–0.69 (m); gel permeation chromatography (GPC): number-average molecular weight (M_n) = 3.2×10^4 g mol^{-1} and polydispersity index (PDI) = 2.3 (against polystyrene standards).

OLED fabrication and measurements

The pre-cleaned ITO glass substrates were treated with ozone for 20 min. Then, the PEDOT:PSS was deposited on the surface of ITO glass by the spin-coating method to form a 40 nm-thick hole-injection layer after being cured at 120 °C for 30 min in the air. The emitting layer (40 nm) was obtained by spin-coating a

chlorobenzene solution of each corresponding phosphorescent polymer. The ITO glass was dried in a vacuum oven at 50 °C for 15 min and it was transferred to the deposition system for organic and metal deposition. TPBi (40 nm), LiF (1 nm) and Al cathode (100 nm) were successively evaporated at a base pressure less than 10^{-6} Torr. The EL spectra and CIE coordinates were measured with a PR650 spectra colorimeter. The *J–V–L* curves of the devices were recorded with a Keithley 2400/2000 source meter and the luminance was measured using a PR650 SpectraScan spectrometer. All the experiments and measurements were carried out under ambient conditions.

Results and discussion

Synthesis and structural characterization

In order to obtain the phosphorescent polymers, three kinds of monomers should be prepared. For the phosphorescent chromophores, they were prepared according to the established two-step strategy by the cyclometalation of $IrCl_3 \cdot nH_2O$ with the corresponding organic ligands prepared by mono-bromination of the concerned triphenylamine derivatives to initially form the μ-chloro-bridged dimers, followed by coordination of the acetylacetone (acac) anion in the presence of [Tl(acac)] under very mild conditions to get the target phosphorescent Ir^{III} complexes **Ir-M1** and **Ir-M2** (Scheme 1). In **Ir-M1** and **Ir-M2**, the functional group of triphenylamine was introduced to afford an HI/HT character to them. The chemical structures of the complexes have been verified by the NMR, mass spectra, *etc.* The ambipolar unit **BP-Br** has been prepared by two step reactions: the Suzuki cross-coupling between 2,5-bis(4-bromophenyl)-1,3,4-oxadiazole and 4-(diphenylamino)phenylboronic acid will get the precompound **BP** (Scheme S1 in the ESI†), which was bromized with NBS to obtain **BP-Br**. In this reaction, there is a possibility to obtain the isomer with dibromo-substitution in the triphenylamine moiety on one side of **BP**. Clearly, the undesired isomer should show much more carbon signals (*ca.* 24 resonance peaks) in its ^{13}C NMR spectrum. However, there are seventeen resonance peaks for the carbon atoms in the ^{13}C NMR spectrum of the obtained product, which is well consistent with the chemical structure of **BP-Br** shown in Scheme 1. So, it can be safely concluded that the obtained product is a pure compound in the form of **BP-Br** rather than a mixture with the undesired isomer aforementioned. This result can be explained as follows: the bromination of **BP** with NBS is an electrophilic substitution reaction. Hence, introducing one bromine group showing electron-withdrawing ability to the triphenylamine moiety will definitely disfavor the substitution of the second one. Furthermore, the reaction is carried out with a weak brominating reagent under very mild conditions to guarantee the good selectivity of the reaction. As a result, pure **BP-Br** with the desired structure can be properly obtained. The ambipolar property of **BP-Br** is afforded by both

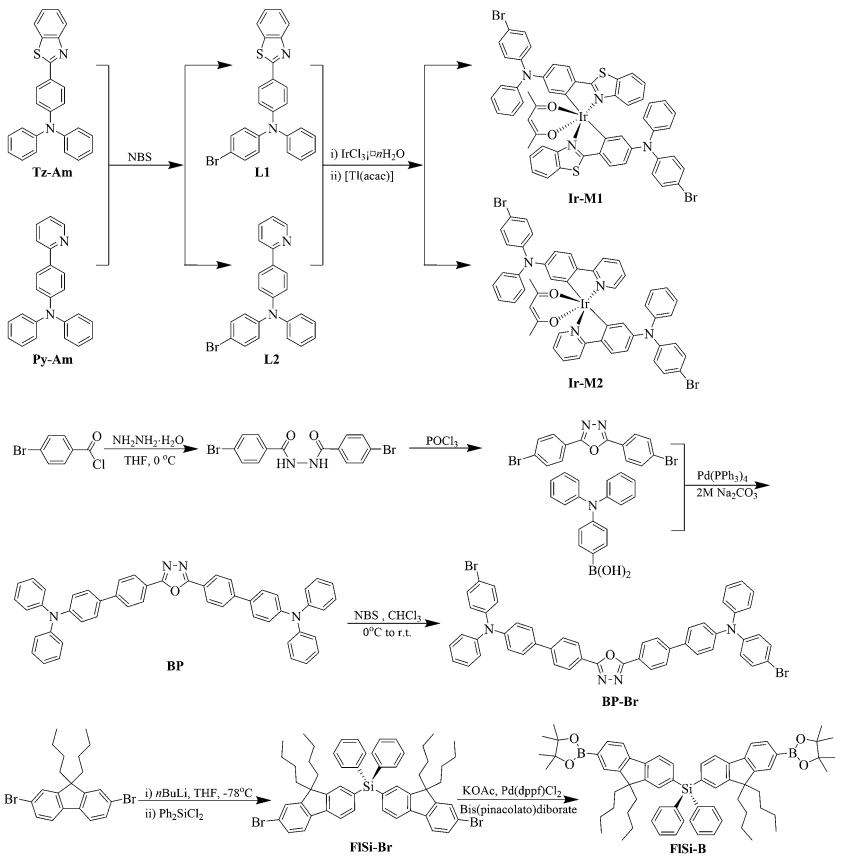

Scheme 1 Synthetic scheme for the monomers required for the synthesis of phosphorescent polymers.

the 1,3,4-oxadiazole ring with the EI/ET property and the triphenylamine moiety with the HI/HT feature. The bromine substituents in **Ir-M1**, **Ir-M2** and **BP-Br** can act as the reaction sites in polymer synthesis. Aromatic silane blocks have been employed to construct host materials for phosphorescent emitters due to their high triplet energy.[43] Hence, fluorene-based silane block **FlSi-B** has been designed with the aim to block the undesired back energy transfer process aforementioned. The **FlSi-B** was synthesized by the cross-coupling between **FlSi-Br** and bis(pinacolato)diborate under base conditions with $Pd(dppf)Cl_2$ as the catalyst. The two pinacol ester groups can afford **FlSi-B** the ability of copolymerization with **Ir-M1**/**Ir-M2** and **BP-Br** to form the designed phosphorescent polymers.

The synthetic procedure for the phosphorescent polymers is shown in Scheme 2. The concerned copolymers were prepared using the Suzuki cross-coupling reaction. According to the inherent character of the phosphorescent system, **Ir-M1** and **Ir-M2** should contribute a small content in the final copolymers to relieve the triplet–triplet (T–T) annihilation effect due to long-lived emissive triplet excited states. So, the weight percentage for **Ir-M1** and **Ir-M2** in the final polymer is controlled less than 10 wt%. Based on the character associated with the copolymerization, the phosphorescent blocks **Ir-M1** and **Ir-M2** can only link with **FlSi-B**, which will make them well scattered along the copolymer backbone to reduce T–T annihilation. This should benefit the EL performance of the phosphorescent polymers. After polymerization, the crude polymer solution was filtered with a 0.45 μm PTFE syringe filter to remove the particles resulting from the decomposition of the $Pd(PPh_3)_4$ catalyst. After concentration, the filtered solution was added to methanol to precipitate the copolymers as colored powders.

The feed ratio of the orange phosphorescent monomer **Ir-M1** was set at 1.58 to 6.35 mol% and the corresponding weight percentage *ca.* 2.0, 4.0, 6.0, and 8.0 wt%. According to the feed ratios of **Ir-M1**, **FlSi-B**, and **BP-Br**, the obtained copolymers are named **P-O-1** (1.58 50 48.42), **P-O-2** (3.27 50 46.73), **P-O-3** (4.95 50 45.05), and **P-O-4** (6.53 50 43.47), respectively (Scheme 2).

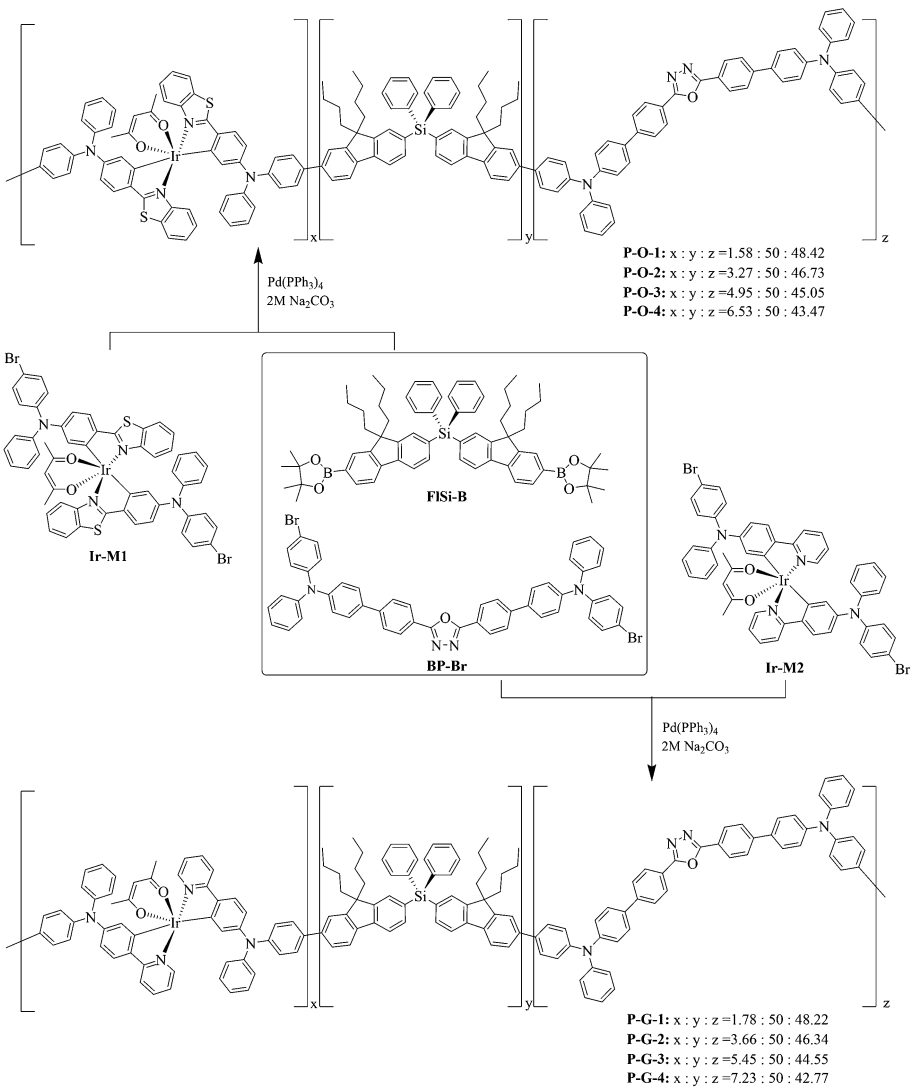

Scheme 2 Synthetic sketch for the phosphorescent polymers.

The synthesis of green phosphorescent copolymers has employed the feed ratio of the **Ir-M2** to retain its weight percentage similar to that of **Ir-M1** with respect to other monomers **FlSi-B** and **BP-Br** (Scheme 2). The resulting copolymers are coded as **P-G-1** (1.78 50 48.22), **P-G-2** (3.66 50 46.34), **P-G-3** (5.45 50 44.55), and **P-G-4** (7.23 50 42.77). In the ^{1}H-NMR spectra of the polymers, the resonance peaks with δ at *ca.* 1.98, 1.10–1.05, and 0.70–0.60 ppm come from the butyl group of the fluorene-based block. The proton signal with δ at 8.20 ppm should be induced by the ambipolar segment, comparing with that of **BP-Br**. Owing to the low content of the phosphorescent moieties, the associated ^{1}H-NMR signals cannot be observed obviously. However, a very weak resonance signal with δ at *ca.* 5.20 and 1.80 ppm can still be detected. This is the characteristic proton signal of the acac anion in the Ir^{III} phosphorescent blocks. All these spectral data have clearly indicated that all the building blocks have been copolymerized together successfully. These phosphorescent polymers are readily soluble in common organic solvents, such as $CHCl_3$, CH_2Cl_2, THF, *etc.* Taking polystyrene as standards, the number average molecular weights (M_n) of the copolymers range from 1.7×10^4 to 3.5×10^4 with polydispersity indices (PDIs) between 1.9 and 2.5.

With the aim to investigate the photophysical and electrochemical properties of the concerned phosphorescent polymers, the model polymers **P-Org** and **P-OSi** are also obtained (Scheme 3). The pure organic polymer **P-Org** was synthesized by the Suzuki cross-coupling between **BP-Br** and **FlSi-B**, while **P-OSi** was prepared by the cross-coupling reaction among **FlSi-B**, **FlSi-Br**, and **Ir-M1** which will correspond for *ca.* 8.0 wt% in **P-OSi**.

Thermal and photophysical properties

The thermal properties of the phosphorescent copolymers have been investigated by thermogravimetric analysis (TGA) and differential scanning calorimetry (DSC) under a nitrogen atmosphere. The TGA results indicate their thermal stability with the 5% weight-reduction temperature ($\Delta T_{5\%}$) ranging from 412 to 398 °C (Table 1). The DSC traces of the copolymers have revealed their high glass-transition temperatures (T_g) in the range from 109 to 120 °C. The good thermal properties of these copolymers will benefit their application in the field of OLEDs.

From Fig. 1, it can be clearly seen that the main absorption bands for the two series copolymers are located before *ca.* 450 nm. It can be safely ascribed to the π–π* transition from both the aromatic silane and ambipolar units. The contribution from the π–π* transition of organic ligands from Ir^{III} phosphorescent chromophores should be inessential due to their low content in the copolymers. However, for the copolymers with higher Ir^{III} phosphorescent chromophore content, such as **P-O-3**, **P-O-4**, and **P-G-4**, inconspicuous absorption bands with very low intensity can be observed in the range from *ca.* 450 nm to 500 nm, which can be assigned to the triplet metal-to-ligand charge transfer (^{3}MLCT) states (Fig. 1 and Table 1). The other copolymers cannot display detectable MLCT absorption bands due the low level of phosphorescent units (Fig. 1 and Table 1).

The photoluminescent (PL) spectra for the phosphorescent copolymers are also investigated in both solution and film states (Fig. S1 in the ESI† and Fig. 2). In CH_2Cl_2 solution, all the copolymers exhibit an emission band at *ca.* 490 nm (Fig. S1† and Table 1). Based on their nanosecond lifetime together with the PL spectra of the copolymer **P-Org** (Table 1 and Fig. S1†), these emission bands should be induced by the pure organic segments in the phosphorescent copolymers. With respect to that in the film state (*ca.* 480 nm, Table 1), the slight bathochromic effect of the high-energy emission band in solution should be induced by the solvent effect of CH_2Cl_2. Differently, these copolymers can show obvious phosphorescent bands in

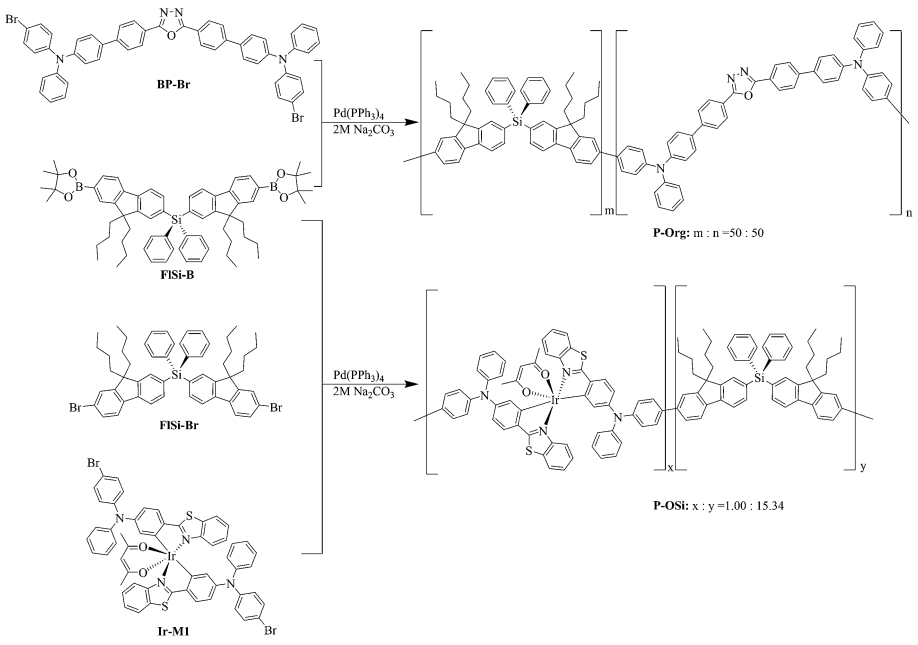

Scheme 3 Synthetic scheme for the polymer of P-Org and P-OSi.

Table 1 Photophysical and thermal-stability data for the concerned polymers

Polymers	Absorption λ_{abs}[a] (nm) 298 K	Emission λ_{em}[b] (nm) 298 K solution/film	τ[c] solution/film	$\Delta T_{5\%}/T_g$ (°C)
P-O-1	292, 305, 318, 356, 382	493/478, 575, 625	2.45 ns/0.88 μs	411/115
P-O-2	292, 304, 317, 356, 383	488/478, 575, 625	2.34 ns/0.80 μs	410/111
P-O-3	292, 303, 318, 355, 382, 483	496/577, 626	2.51 ns/0.78 μs	408/110
P-O-4	292, 305, 318, 356, 382, 483	490/577, 625	2.40 ns/0.74 μs	398/110
P-G-1	296, 326, 358, 380	498/478, 526	2.55 ns/0.19 μs	412/109
P-G-2	394, 319, 356, 380	499/480, 530, 574	2.51 ns/0.15 μs	410/120
P-G-3	300, 312, 325, 375	493/480, 533, 573	2.42 ns/0.20 μs	405/120
P-G-4	297, 325, 358, 380, 458	499/478, 533, 573	2.55 ns/0.16 μs	403/113
P-Org	292, 316, 356, 380	490/480	2.51 ns/—	415/118

[a] Measured in CH_2Cl_2 at a concentration of 0.02 mg mL^{-1}. [b] Measured in CH_2Cl_2 at a concentration of 0.02 mg mL^{-1}. [c] For the solution samples, the lifetime (τ) was referred to the emission band at *ca.* 490 nm. For the film samples, the τ was assigned to the phosphorescent band. The excitation wavelength for the measure was set at 400 nm.

the film state. The phosphorescent emission bands of the copolymer films generally are enhanced by increasing the content level of phosphorescent units (Fig. 2). However, the phosphorescent intensity shows a slight decrease at high contents of the Ir^{III} complex blocks (**P-O-4** and **P-G-4**) (Fig. 2), which should be induced by the weak quenching effect among the phosphorescent units. For **P-O-1–P-O-4**, the high-energy emission band almost disappears (Fig. 2a) due to the efficient energy-transfer from the pure organic segments to the phosphorescent units, which is typically shown in phosphorescent polymers. Different from **P-O-1–P-O-4**, the copolymers **P-G-1–P-G-4** can still show obvious high-energy emission bands at *ca.* 480 nm besides the phosphorescent ones (Fig. 2b), indicating

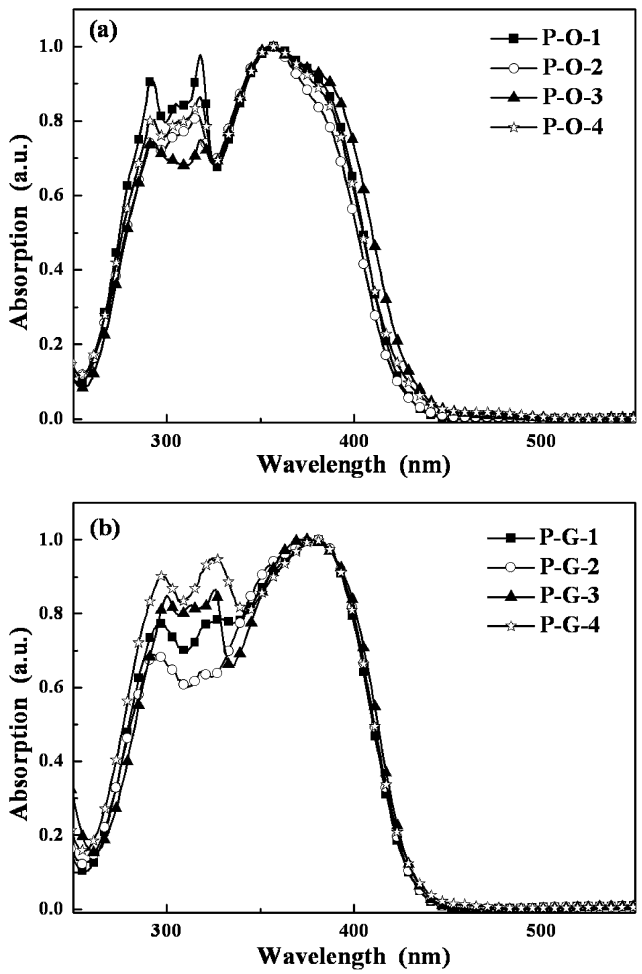

Fig. 1 UV-vis spectra for the phosphorescent polymers. (a) P-O-1–P-O-4 and (b) P-G-1–P-G-4.

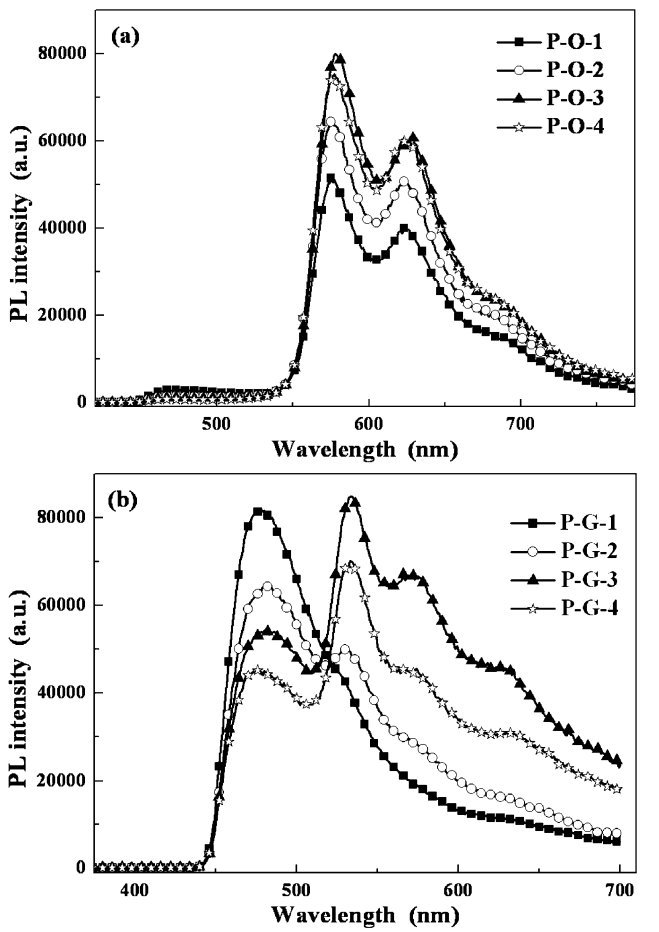

Fig. 2 The PL spectra for the film of the phosphorescent copolymers at 298 K.

the inefficient energy-transfer process. In order to explain this issue, the UV-vis spectra for the organic copolymer **P-Org** and the Ir^{III} monomers (**Ir-M1** and **Ir-M2**) have been obtained (Fig. 3). Under the excitation wavelength of 390 nm, the organic ligands of the Ir^{III} monomers can be excited based on their absorption spectra (Fig. 3). The photophysical properties of the organic segments formed between **BP-Br** and **FlSi-B** in the polymer backbones should be similar to that of **P-Org** due to the low content of the Ir^{III} monomers. The ratiocination has been confirmed by the great resemblance between their UV-vis, PL, and lifetime (Table 1, Fig. 1, 3 and S1†). Hence, the photophysical property of **P-Org** can be safely employed to represent those of the organic segments in the polymer backbones. According to the UV-vis spectrum of **P-Org** in Fig. 3, the 390 nm light can induce the excitation of organic segments in the phosphorescent polymers as well. For **P-O-1–P-O-4**, the energy-level for the first singlet states (S_1') of their organic segments is higher than that for the first singlet states (S_1^O) of the organic ligands in **Ir-M1** (Fig. 3). There should be a cascade energy-transfer process from S_1' to S_1^O, then from S_1^O to $^1MLCT^O$ (singlet states of MLCT in **Ir-M1**), which is converted *via* inter-system crossing (ISC) into emissive $^3MLCT^O$ (triplet states of MLCT in **Ir-M1**) (Fig. 4a) to induce phosphorescence signals in the polymers of **P-O-1–P-O-4** (Fig. 2a). According to the energy-level involved, the energy-transfer process in **P-O-1–P-O-4** is an energy-favored down-hill procedure to guarantee its high efficiency (Fig. 4a). Additionally, there is good over-lap between the absorption spectrum of **Ir-M1** and the PL spectrum of **P-Org** (Fig. 3), indicating the facilitation of the energy-transfer from the organic segments to phosphorescent units in **P-O-1–P-O-4**. Hence, the highly efficient cascade energy-transfer process should greatly reduce the chance for the decay of S_1' to the ground state (S_o). Accordingly, there is almost no high-energy fluorescent emission bands associated with the transition of S_1' to S_o in the film of **P-O-1–P-O-4** (Fig. 2a). However, polymers **P-G-1–P-G-4** should show a different situation. According to Fig. 3, the S_1' states show almost the same energy level to that of the first singlet states (S_1^G) of the organic ligands in **Ir-M2**. So, there is resonance energy-transfer between the S_1' and S_1^G states (Fig. 4b). Obviously, the resonance

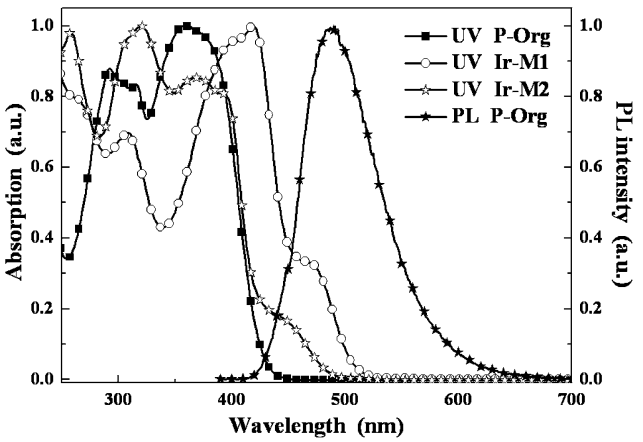

Fig. 3 UV-vis spectra for P-Org, Ir-M1 and Ir-M2 together with the PL spectrum of P-Org in CH_2Cl_2 at 298 K.

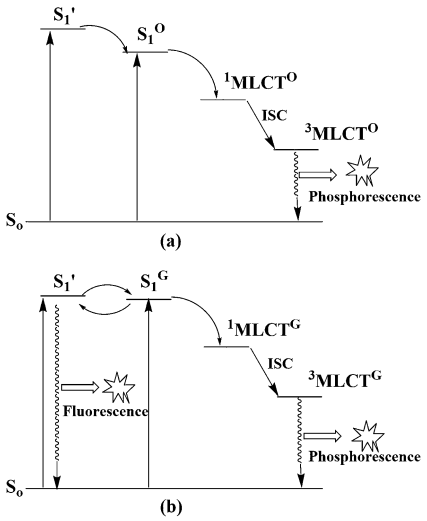

Fig. 4 energy-transfer process involved in the phosphorescent polymers. (a) P-O-1–P-O-4 and (b) P-G-1–P-G-4.

procedure will not only increase the chance for the decay of the radiative S_1' to S_o to induce high-energy fluorescence bands, but also render ineffectiveness to the cascade energy-transfer process from S_1' to S_1^G, then from S_1^G to $^1MLCT^G$ (singlet states of MLCT in **Ir-M2**). As a result, the emission from $^3MLCT^G$ (triplet states of MLCT in **Ir-M2**) will decrease, which will weaken the phosphorescent signal in **P-G-1–P-G-4**. Furthermore, the over-lap between the absorption spectrum of **Ir-M2** and the PL spectrum of **P-Org** is poor (Fig. 3), disfavoring the energy-transfer from the organic segments to phosphorescent units in **P-G-1–P-G-4**. As a result, both fluorescence and phosphorescence bands can be observed in the film of **P-G-1–P-G-4** (Fig. 2b). Different from electrical excitation, photoexcitation typically generates singlet states. Furthermore, with excitation at 390 nm, both the ^3MLCT of phosphorescent units and the triplet states of the organic segments in the polymers cannot be formed directly through the photoexcitation. Hence, the triplet energy-transfer among the triplet states might be ruled out in the polymer films under photoexcitation.

Electrochemical characterization

Under a nitrogen atmosphere, the electrochemical behavior of these phosphorescent polymers was characterized by the cyclic voltammetry (CV) measurements calibrated with ferrocene (Fc) as the internal standard. In order to evaluate the effect of the ambipolar moiety on the charge carrier injection ability of the copolymers, the CV characterization for **P-Org** and **P-OSi** was also conducted. The polymers **P-O-1–P-O-4** and **P-G-1–P-G-4** all show an reversible oxidation process at *ca.* 0.5 V ranging from 0.49 V to 0.55 V (Table 2). Similarly, these polymers also show alike reduction potential at *ca.* −2.5 V (Table 2). With the aim to assign the oxidation and reduction processes, these data are compared with those of **P-Org** and **P-OSi**. It can be clearly seen that the CV data of **P-Org** with $E_{1/2}^{ox}$ at *ca.* 0.5 V and $E_{1/2}^{red}$ at *ca.* −2.50 V are very similar to those of the phosphorescent

Table 2 Redox properties of the polymers

Copolymers	$E_{1/2}^{ox}$ (V)	$E_{1/2}^{red}$ [a] (V)	E_{HOMO} (eV)	E_{LUMO} (eV)
P-O-1	0.53	−2.48	−5.33	−2.32
P-O-2	0.55	−2.43	−5.35	−2.37
P-O-3	0.52	−2.45	−5.32	−2.35
P-O-4	0.55	−2.45	−5.35	−2.35
P-G-1	0.49	−2.51	−5.29	−2.29
P-G-2	0.50	−2.55	−5.30	−2.25
P-G-3	0.53	−2.47	−5.33	−2.33
P-G-4	0.49	−2.49	−5.29	−2.31
P-Org	0.47	−2.50	−5.27	−2.30
P-OSi	1.05	—	−5.85	—

[a] Irreversible.

polymers. So, it can be concluded that the oxidation and reduction processes in the phosphorescent polymers are induced by their organic segments, composed of aromatic silane and the ambipolar moieties. It indicates that the CV signal associated with the Ir^{III} phosphorescent units cannot be properly detected, which should be due to their low content in the corresponding polymers. Without the ambipolar moiety, **P-OSi** shows a noticeably different CV behavior from the other polymers with much higher $E_{1/2}^{ox}$ at *ca.* 1.05 V and no detectable reduction process in the scan potential range (Table 2). Taking all the results into consideration, the oxidation and reduction processes of the concerned phosphorescent copolymers should come from the ambipolar moieties in their backbone. The electron-rich triphenylamine group in the ambipolar moiety induces the oxidation process of the phosphorescent polymers and the electron-deficient oxadiazole unit will be responsible for their reduction process. Comparing the CV behaviors between **P-OSi** and the concerned phosphorescent polymers, it can be clearly seen that introducing ambipolar moieties can effectively improve the injection ability for both kinds of charge carriers of the concerned phosphorescent polymers. This should benefit the EL performance of the investigated copolymers.

Electroluminescent properties

Inspired by their charge carrier injection/transporting properties, these polymers were employed as emitters to construct phosphorescent OLEDs (PHOLEDs) to evaluate their electroluminescent properties. These phosphorescent polymers are very soluble in common organic solvents such as chloroform, THF, toluene, chlorobenzene, *etc.* and thus the concerned PHOLEDs are fabricated with a solution-processing approach. The device configuration was ITO/PEDOT:PSS (40 nm)/emission layer, EML (40 nm)/TPBi (40 nm)/LiF (1 nm)/Al (100 nm). Fig. 5 depicts the structure of the multi-layer PHOLEDs and the chemicals involved in the fabrication of the devices. The PEDOT:PSS layer was firstly deposited by spin-coating on the pre-cleaned ITO surface to form a hole-injection layer (HIL) for its matching HOMO level with that of ITO. The emission layer (EML) is constructed on the PEDOT:PSS layer by spin-coating the

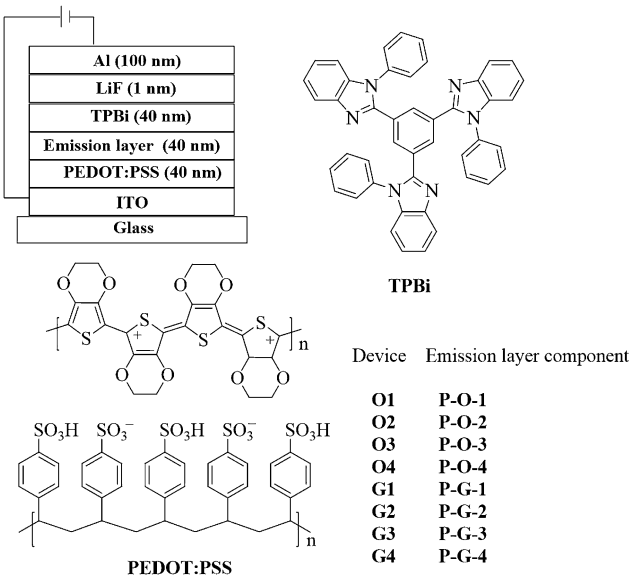

Fig. 5 The configuration of the PHOLEDs made from the phosphorescent polymers and the chemical structures for the involved functional materials.

chlorobenzene solution of the concerned phosphorescent polymer. Similar to their analogs, the organic segments in the polymer backbone will act as the host material for the phosphorescent Ir^{III} complex moieties. The 1,3,5-tris(1-phenyl-1*H*-benzo[*d*]imidazol-2-yl)benzene (TPBi) layer plays the role of both hole-blocking and electron-transporting, while LiF acts as an electron-injection layer.

When the proper voltage was applied to the PHOLEDs, intense electrophosphorescence can be observed. For devices **O1–O4**, they show orange EL representing line-shapes similar to that of the corresponding polymers in the film state, indicating that the origin of EL is from the phosphorescent units (Fig. 6). There is only a very weak EL band from organic segments in the polymers for devices **O1** and **O2** due to the low level of the phosphorescent units which cannot take in all the energy

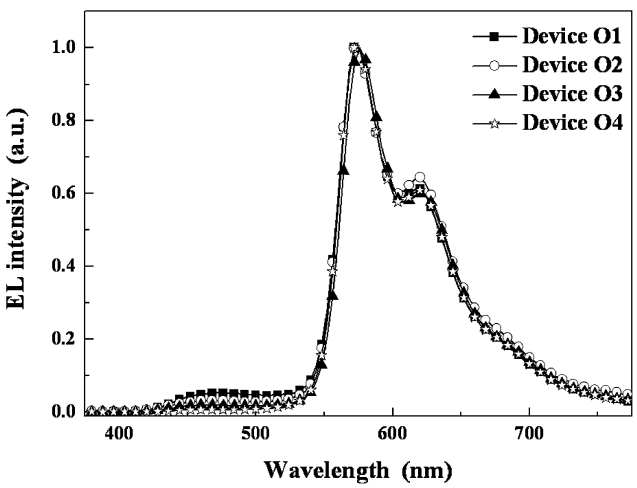

Fig. 6 The EL spectra for the devices **O1–O4** at *ca.* 12 V.

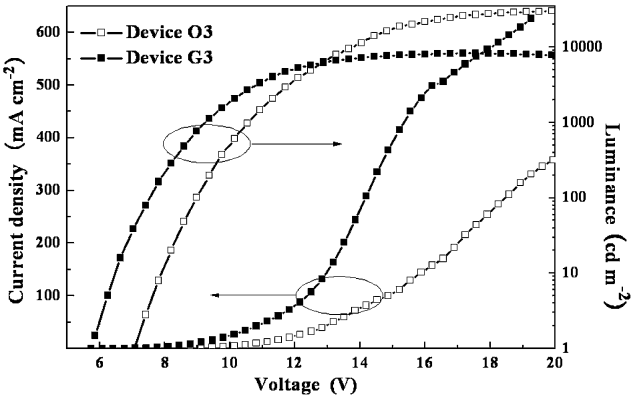

Fig. 7 The *J–V–L* curves for the optimized devices **O3** and **G3**.

transferred from the organic segments in the polymers. Importantly, the undesired EL band vanishes in devices **O3** and **O4** made from polymers (**P-O-3** and **P-O-4**, respectively) with the higher level of the phosphorescent units, showing the complete energy-transfer from the host (organic segments) to the guests (phosphorescent units). Differently, for devices **G1–G4**, there is an obvious EL band from organic segments even for the device **G4** made from the polymer **P-G-4**, a high level of the phosphorescent units besides the green EL band from iridium complex moieties (Fig. S2 in the ESI†). With respect to that of devices **O1–O4**, devices **G1–G4** show the much inefficient host–guest energy-transfer process, which can be ascribed to the resonance energy-transfer between S_1' and S_1^G states as shown before (Fig. 4b).

The current–density–voltage–luminance (*J–V–L*) curves for the PHOLEDs are shown in Fig. 7 and S3,† and the corresponding EL data are summarized in Table 3. Compared with the other devices emitting orange color, device **O3** can show the maximum EL abilities with a peak luminance (L_{max}) of 30 532 cd m^{-2} at 18.4 V, a current efficiency (η_L) of 30.54 cd A^{-1}, an external quantum efficiency (η_{ext}) of 12.93% and a power efficiency (η_P) of 10.12 lm W^{-1}. Besides device **O3**, device **O2** can also furnish attractive EL performance with an L_{max} of 18 148 cd m^{-2} at 16.9 V, 27.46 cd A^{-1}, 11.91% and 9.82 lm W^{-1}, respectively, (Table 3 and Fig. S4 in the ESI†). However, compared with the orange-emitting analogs, the green-emitting PHOLEDs show noticeably poorer EL abilities. For the optimized device **G3**, it exhibits peak EL performance with an L_{max} of 8305 cd m^{-2} at 15.4 V, a η_L of 13.25 cd A^{-1}, a η_{ext} of 5.07% and a η_P of 5.19 lm W^{-1}. The proper explanation for the difference between the two series of PHOLEDs can be as follows: clearly, the energy-transfer from the organic segments (host) to the phosphorescent units (guest) is much more efficient in the EL process associated with devices **O1–O4** compared with that involved in devices **G1–G4**, indicated by the obvious EL band in the short wavelength region for the EL spectra of devices **G1–G4** (Fig. S2 in the ESI†). The EL band from the organic segments will indicate the formation of the nonemissive triplet excitons, which may give no contribution to the EL of the devices **G1–G4** and will lower their EL efficiencies accordingly. Furthermore, the low-temperature PL spectrum for **P-Org** has indicated that the triplet energy-level for the organic segment is *ca.* 2.23 eV, which is lower than the triplet energy-level of *ca.* 2.33 eV for the green phosphorescent units in **P-G-1–P-G-4** (Fig. S5†). It means that there will be

Table 3 The EL performance of the PHOLEDs

Device	Polymers	$V_{turn\text{-}on}$ (V)	Luminance L_{max}[a] (cd m^{-2})	η_{ext} (%)	η_L (cd A^{-1})	η_p (lm W^{-1})	λ_{max}[d] (nm)
O1	**P-O-1**	5.1	12 695 (13.9)	8.10 (8.1)[a]	19.35 (7.8)	7.82 (7.8)	572
				6.74[b]	16.17	6.27	(0.52, 0.44)
				4.15[c]	9.94	2.89	
O2	**P-O-2**	5.7	18 148 (16.9)	11.91 (8.8)	27.46 (8.8)	9.82 (8.8)	572
				11.27	26.03	8.64	(0.53, 0.44)
				5.45	12.05	2.95	
O3	**P-O-3**	6.7	30 532 (18.4)	12.93 (10.6)	30.54 (10.6)	10.12 (8.6)	576
				12.68	30.06	8.34	(0.54, 0.44)
				9.71	23.0	5.03	
O4	**P-O-4**	5.4	13 812 (16.6)	9.52 (8.1)	23.11 (8.1)	9.79 (7.1)	572
				8.75	21.22	7.05	(0.54, 0.44)
				4.50	10.83	2.65	
G1	**P-G-1**	7.0	2516 (19.1)	1.36 (8.6)	2.68 (8.6)	1.04 (6.3)	488, 532
				0.95	1.87	0.41	(0.32, 0.41)
				0.61	1.20	0.23	
G2	**P-G-2**	6.4	8824 (15.2)	1.29 (11.5)	3.40 (11.5)	1.86 (9.5)	488, 536
				1.13	2.98	1.88	(0.38, 0.49)
				1.27	3.37	1.74	
G3	**P-G-3**	5.7	8305 (15.4)	5.07 (8.6)	13.25 (8.6)	5.19 (7.6)	488, 536
				4.95	12.88	4.35	(0.44, 0.50)
				2.49	6.50	1.70	
G4	**P-G-4**	7.4	7184 (18.5)	3.97 (8.0)	8.98 (8.0)	3.56 (7.7)	488, 536
				2.72	6.16	1.61	(0.44, 0.51)
				1.87	4.24	0.88	

[a] Maximum values of the devices. Values in parentheses are the voltage at which they were obtained. [b] Values were collected at 20 mA cm^{-2}. [c] Values collected at 100 cd m^{-2}. [d] The CIE coordinates (*x*, *y*) are shown in parentheses.

undesired back energy-transfer from the emissive triplet states of the green phosphorescent units to the nonemissive triplet states of the organic segments in the EL process of the devices **G1–G4**, which will definitely disfavor the EL performance of the concerned devices. So, taking all of these into consideration, it is will be easy to interpret the inferior EL performance of devices **G1–G4**. Despite these disadvantages, device **G3** can still show decent EL efficiencies for polymer PHOLEDs, which might be ascribed to both the ambipolar feature and functionalizing of the phosphorescent units of the polymers. However, the situation in the devices **O1–O4** should be different. Only a very weak EL band from organic segments can be observed in the devices **O1** and **O2**, indicating much less nonemissive triplet excitons of the organic segments formed in the devices **O1–O4**. Critically, the energy-level for these undesired triplet excitons (*ca.* 2.23 eV) is higher than that of the orange phosphorescent units in **P-O-1–P-O-4** (*ca.* 2.15 eV), which are derived from their low temperature PL spectra (Fig. S5†). Hence, despite that these nonemissive triplet excitons are formed, they will be harnessed easily by the emissive triplet excitons of the orange phosphorescent units in **P-O-1–P-O-4** through cascade energy-transfer to contribute the EL of the devices **O1–O4**. As a result, devices **O1–O4** can outperform their analogous devices **G1–G4** (Table 3).

Generally, most of the phosphorescent polymers show relatively low EL efficiency with η_L less than 10 cd A^{-1}. Encouragingly, some advanced phosphorescent polymers can also bring high EL efficiencies. Some functionalized blue-emitting phosphorescent polymers with a phosphine oxide ether backbone can show a η_L of 19.4 cd A^{-1}.[27] The phosphorescent polymers with nonconjugated backbones attached with blue-emitting Ir^{III} dendrons can achieve a η_L of 28.1 cd A^{-1}.[17] Attaching green-emitting Ir^{III} complexes to the carbazole-based backbone can also bring highly efficient phosphorescent polymers which can be employed to make PHOLEDs with an excellent η_L of 33.9 cd A^{-1}.[15] Novel polyfluorene-based phosphorescent polymers have also been developed with a red-emitting Os^{II} complex as the phosphorescent unit, triphenylamine as the pendent hole transporting group, and oxadiazole as the electron transporting pendent moiety. These highly efficient red phosphorescent polymers can achieve a high η_L of 26.3 cd A^{-1}.[21] Besides all these high performance phosphorescent polymers, the carbazole-based silane moiety has also been employed to construct a polymer backbone grafted with a blue-emitting Ir^{III} complex (FIrpic).[19] The concerned phosphorescent polymers can furnish a η_L of 2.3 cd A^{-1}. To compare with these attractive EL efficiencies reported, the optimized device **O3** made from **P-O-3** can achieve a competitive η_L of 30.54 cd A^{-1}. Even for the device **G3** bothered by the undesired back energy-transfer, it can also maintain a maximum η_L of 13.25 cd A^{-1}, representing the state-of-the-art EL efficiencies ever achieved by phosphorescent polymers. These EL data have clearly indicated the great potential of these novel phosphorescent polymers in PHOLEDs.

The EL efficiency–current density curves for the PHOLEDs are given in Fig. 8 and S4.† From these figures, it can clearly be seen that the undesired EL efficiency roll-off effect is unserious for the concerned PHOLEDs, indicating very slight T–T annihilation involved. This result might be ascribed to the contorted configuration associated with both fluorene-based silane units and phosphorescent moieties, which will afford twisted backbones to the concerned polymers. The twisted polymer backbones will make the phosphorescent moieties keep away from each other to relieve the T–T annihilation effect. All these encouraging EL data have obviously shown the importance of the involved molecular design conception, which will construct a new platform for the design and synthesis of high-performance phosphorescent polymers.

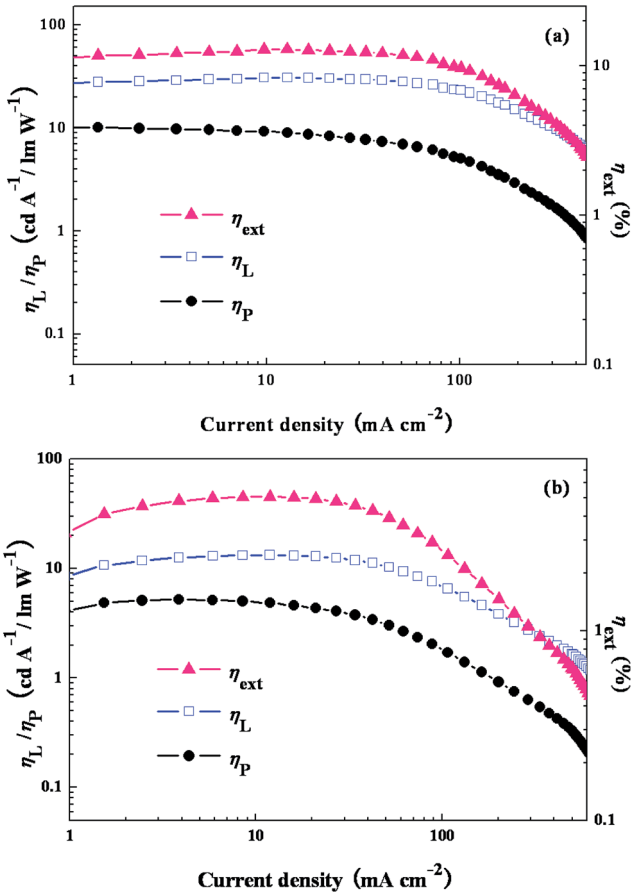

Fig. 8 The dependence of EL efficiencies on the current density for (a) device O3 and (b) device G3.

Conclusions

Novel phosphorescent polymers have been successfully developed by Suzuki cross-coupling among the functionalized monomers with the aim to deal with the drawbacks associated with the traditional analogues. Both functionalized phosphorescent Ir^{III} ppy-type complex units and ambipolar blocks together with flourene-based silane moieties have been employed to optimize the opt-electronic characters of the corresponding polymers. The great potential of this strategy has been indicated by the high EL efficiencies of the OLEDs made from these phosphorescent polymers, showing a maximum current efficiency (η_L) of 30.54 cd A^{-1}, an external quantum efficiency (η_{ext}) of 12.93% and a power efficiency (η_P) of 10.12 lm W^{-1}. Clearly, the results will reveal important information for the design and synthesis of new highly efficient phosphorescent polymers.

Acknowledgements

This work was financially supported by Tengfei Project from Xi'an Jiaotong University, the Fundamental Research Funds for the Central Universities, the Program for New Century Excellent Talents in University, theMinistry of Education of China (NECT-09-0651), the Key Creative Scientific Research Team in Shaanxi Province (2013KCT-05), the China Postdoctoral Science Foundation (Grant no. 20130201110034), and the National Natural Science Foundation of China (no. 20902072).

Notes and references

1 H. Wu, L. Ying, W. Yang and Y. Cao, *Chem. Soc. Rev.*, 2009, **38**, 3391.
2 X. Yang, G. Zhou and W.-Y. Wong, *J. Mater. Chem. C*, 2014, **2**, 1760.
3 S. Gong, C. Yang and J. Qin, *Chem. Soc. Rev.*, 2012, **41**, 4797.
4 X. Chen, J.-L. Liao, Y. Liang, M. O. Ahmed, H.-E. Tseng and S.-A. Chen, *J. Am. Chem. Soc.*, 2003, **125**, 636.
5 A. J. Sandee, C. K. Williams, N. R. Evans, J. E. Davies, C. E. Boothby, A. Köhler, R. H. Friend and A. B. Holmes, *J. Am. Chem. Soc.*, 2004, **126**, 7041.
6 X. Gong, M. R. Robinson, J. C. Ostrowski, D. Moses, G. C. Bazan and A. J. Heeger, *Adv. Mater.*, 2002, **14**, 581.
7 P. A. Lane, L. C. Palilis, D. F. O'PBrien, C. Giebeler, A. J. Cadby, D. G. Lidzey, A. J. Campbell, W. Blau and D. D. C. Bradley, *Phys. Rev. B: Condens. Matter Mater. Phys.*, 2001, **63**, 5206.
8 G. Zucchi, D. Tondelier, Y. Bonnassieux and B. Geffroy, *Polym. Int.*, 2014, **63**, 1368.
9 J. Jiang, C. Jiang, W. Yang, H. Zhen, F. Huang and Y. Cao, *Macromolecules*, 2005, **38**, 4072.
10 P. I. Lee, S. L. C. Hsu and J. F. Lee, *J. Polym. Sci., A: Polym. Chem.*, 2008, **46**, 464.
11 K. Zhang, Z. Chen, C. Yang, Y. Tao, Y. Zou, J. Qin and Y. Cao, *J. Mater. Chem.*, 2008, **18**, 291.
12 F. I. Wu, X. H. Yang, D. Neher, R. Dodda, Y. H. Tseng and C. F. Shu, *Adv. Funct. Mater.*, 2007, **17**, 1085.
13 J. X. Jiang, Y. H. Xu, W. Yang, R. Guan, Z. Q. Liu, H. Y. Zhen and Y. Cao, *Adv. Mater.*, 2006, **18**, 1769.
14 D. A. Poulsen, B. J. Kim, B. Ma, C. S. Zonte and J. M. J. Fréchet, *Adv. Mater.*, 2009, **21**, 77.
15 Z. Ma, L. Chen, J. Ding, L. Wang, X. Jing and F. Wang, *Adv. Mater.*, 2011, **23**, 3726.
16 J. H. Park, T.-W. Koh, J. Chung, S. H. Park, M. Eo, Y. Do, S. Yoo and M. H. Lee, *Macromolecules*, 2013, **46**, 674.
17 W.-Y. Lai, J. W. Levell, M. N. Balfour, P. L. Burn, S.-C. Lo and I. D. W. Samuel, *Polym. Chem.*, 2012, **3**, 734.
18 J. Yu, Y. Wang, Y. Liu, X. Deng, H. Tan, Z. Zhang, M. Zhu and W. Zhu, *J. Organomet. Chem.*, 2014, **761**, 51.
19 T. Fei, G. Cheng, D. Hu, W. Dong, P. Lu and Y. Ma, *J. Polym. Sci., A: Polym. Chem.*, 2010, **48**, 1859.
20 Q. Chen, N. Liu, L. Ying, W. Yang, H. Wu, W. Xu and Y. Cao, *Polymer*, 2009, **50**, 1430.
21 C. H. Chien, S. F. Liao, C. H. Wu, C. F. Shu, S. Y. Chang, Y. Chi, P. T. Chou and C. H. Lai, *Adv. Funct. Mater.*, 2008, **18**, 1430.
22 G. L. Schulz, X. Chen, S.-A. Chen and S. Holdcroft, *Macromolecules*, 2006, **39**, 9157.
23 H. Zhen, C. Jiang, W. Yang, J. Jiang, F. Huang and Y. Cao, *Chem.–Eur. J.*, 2005, **11**, 5007.
24 (*a*) K. Zhang, Z. Chen, C. Yang, Y. Zou, S. L. Gong, J. Qin and Y. Cao, *J. Phys. Chem. C*, 2008, **112**, 3907; (*b*) K. Zhang, Z. Chen, C. Yang, S. Gong, J. Qin and Y. Cao, *Macromol. Rapid Commun.*, 2006, **27**, 1926; (*c*) K. Zhang, Z. Chen, Y. Zou, C. Yang, J. Qin and Y. Cao, *Organometallics*, 2007, **26**, 3699.
25 W. Zhang, H. Jin, F. Zhou, Z. Shen, D. Zou and X. Fan, *J. Polym. Sci., A: Polym. Chem.*, 2012, **50**, 3895.
26 S. Shao, J. Ding, L. Wang, X. Jing and F. Wang, *J. Am. Chem. Soc.*, 2012, **134**, 20290.
27 S. Shao, J. Ding, L. Wang, X. Jing and F. Wang, *J. Am. Chem. Soc.*, 2012, **134**, 15189.
28 S. Shao, J. Ding, L. Wang, X. Jing and F. Wang, *J. Mater. Chem.*, 2012, **22**, 24848.
29 A. P. Monkman, H. D. Burrows, L. J. Hartwell, L. E. Horsburgh, I. Hamblett and S. Navaratnam, *Phys. Rev. Lett.*, 2001, **86**, 1358.
30 G.-J. Zhou, C.-L. Ho, W.-Y. Wong, Q. Wang, D. Ma, L. Wang, Z. Lin, T. B. Marder and A. Beeby, *Adv. Funct. Mater.*, 2008, **18**, 499.
31 W.-Y. Wong, G.-J. Zhou, X.-M. Yu, H.-S. Kwok and B.-Z. Tang, *Adv. Funct. Mater.*, 2006, **16**, 838.
32 G. Zhou, W.-Y. Wong, B. Yao, Z. Xie and L. Wang, *Angew. Chem., Int. Ed.*, 2007, **46**, 1149.
33 X. Xu, X. Yang, J. Dang, G. Zhou, Y. Wu, H. Li and W.-Y. Wong, *Chem. Commun.*, 2014, **50**, 2473.
34 X. Yang, N. Sun, J. Dang, Z. Huang, C. Yao, X. Xu, C.-L. Ho, G. Zhou, D. Ma, X. Zhao and W.-Y. Wong, *J. Mater. Chem. C*, 2013, **1**, 3317.
35 W.-Y. Wong, C.-L. Ho, Z.-Q. Gao, B.-X. Mi, C.-H. Chen, K.-W. Cheah and Z. Lin, *Angew. Chem., Int. Ed.*, 2006, **45**, 7800.
36 J. Ding, B. Wang, Z. Yue, B. Yao, Z. Xie, Y. Cheng, L. Wang, X. Jing and F. Wang, *Angew. Chem., Int. Ed.*, 2009, **48**, 6664.
37 G.-J. Zhou, Q. Wang, C.-L. Ho, W.-Y. Wong, D. Ma, L. Wang and Z. Lin, *Chem.–Asian J.*, 2008, **3**, 1830.
38 Y. T. Tao, C. L. Yang and J. G. Qin, *Chem. Soc. Rev.*, 2011, **40**, 2943.
39 Y. T. Tao, Q. Wang, C. L. Yang, Q. Wang, Z. Q. Zhang, T. T. Zou, J. G. Qin and D. G. Ma, *Angew. Chem., Int. Ed.*, 2008, **47**, 8104.
40 Y. Tao, Q. Wang, L. Ao, C. Zhong, J. Qin, C. Yang and D. Ma, *J. Mater. Chem.*, 2010, **20**, 1759.
41 H.-Y. Wang, G. Chen, X.-P. Xu and S.-J. Ji, *Synth. Met.*, 2010, **160**, 1065.
42 G. Zhou, Y. He, B. Yao, J. Dang, W.-Y. Wong, Z. Xie, X. Zhao and L. Wang, *Chem.–Asian J.*, 2010, **5**, 2405.
43 G. Cheng, T. Fei, Y. Duan, Y. Zhao, Y. Ma and S. Liu, *Opt. Lett.*, 2010, **35**, 2436.